Chemical Science

EDGE ARTICLE

View Article Online
View Journal | View Issue

Cite this: *Chem. Sci.*, 2018, **9**, 2480

Effect of ion migration in electro-generated chemiluminescence depending on the luminophore types and operating conditions†

Sangbaie Shin,[a] Yun Sung Park,[b] Sunghwan Cho,[c] Insang You,[a] In Seok Kang,[b] Hong Chul Moon *[d] and Unyong Jeong *[a]

Received 12th September 2017
Accepted 26th January 2018

DOI: 10.1039/c7sc03996d

rsc.li/chemical-science

Electro-generated chemiluminescence (ECL) has attracted increasing attention as a new platform for light-emitting devices; in particular, the use of mechanically stretchable ECL gels opens up the opportunity to achieve deformable displays. The movements of radical ions under an external electric field include short-range diffusion near the electrodes and long-distance migration between the electrodes. So far, only the diffusion of radical ions has been considered as the operating principle behind ECL. In this study, electrochemical and optical analysis was performed systematically to investigate the role of ion migration in ECL devices. This study reveals that long-distance migration of radical ions can be a key variable in ECL at low frequencies and that this effect depends on the type of ion species and the operating conditions (*e.g.* voltage and frequency). We also report that the emissions from the two electrodes are not identical, and the emission behaviors are different in the optimal operating conditions for the red, green, and blue ECL emissions.

Introduction

Electro-generated chemiluminescence (ECL) refers to light emission *via* electrochemical reactions of a luminophore (A) near an electrode surface.[1–7] Upon the application of alternating current (AC), oxidized and reduced radical ions are generated at the electrodes. When the concentration profiles of these two species encounter each other, thermodynamically spontaneous electron transfer reactions occur, resulting in the production of excited-state luminophores (A*). This ECL process corresponds to the annihilation pathway. A remarkable feature of an ECL display is its simple device structure, which is composed of only a light-emitting layer between the top and bottom electrodes without the electron and hole transporting layers. Furthermore, ECL displays do not require careful adjustment of the work function between the light-emitting layer and the electrodes.[8] They are less sensitive to moisture compared to organic light-emitting diodes.[9] Several variants of ECL displays have been demonstrated. Solid-type ECL devices have a long response time due to the relatively slow ion mobility.[10–13] Solution-type ECL devices face issues such as solvent evaporation and material leakage.[14–18] On the other hand, gel-type ECL devices address such problems and have additional advantages such as mechanical flexibility and stretchability.[8,19–22] Therefore, gel-type ECL displays have been of great interest as simple deformable next-generation displays.

The conventional concept of diffusion-dominant electrochemistry makes a lot of electrolyte systems tractable – particularly when aspects of the reactivity of the ECL luminophores are under study. However, this simplified concept sometimes fails to clearly explain experimental observations. In the absence of convective flow, the mass transport of an ion species can arise because of an electrochemical potential gradient formed over a given distance. The concentration gradient of the ion typically causes short-distance diffusion and the electrochemical potential gradient induces long-distance movement (electro-migration).[23] The conventional concept behind ECL devices assumes that the long-distance movement of the electro-active ion can be neglected in the presence of excess supporting electrolytes. This assumption is based on the calculation stating that the number of long-distance migrating ions contributing to the current is negligible compared to the number of diffusive active ions contributing to the current.[3] However, the concept decoupling the diffusion current from the migration current is not scientifically reasonable because each ion is influenced by a combined electrochemical potential caused by the concentration gradient and the electric potential gradient. The electric field may enhance the directional linear

[a]*Department of Materials Science and Engineering, Pohang University of Science, Pohang 37673, Korea. E-mail: ujeong@postech.ac.kr*

[b]*Department of Chemical Engineering, Pohang University of Science, Pohang 37673, Korea*

[c]*Department of Materials Science Engineering, Yonsei University, Seoul, 03722, Korea*

[d]*Department of Chemical Engineering, University of Seoul, Seoul 02504, Korea. E-mail: hcmoon@uos.ac.kr*

† Electronic supplementary information (ESI) available. See DOI: 10.1039/c7sc03996d

diffusion, which would then increase the linear velocity of the ions.

In addition, the dynamic electric field (*i.e.*, AC voltage) induces unsteady-state mass transfer, which is different from the steady-state assumption in the conventional calculation of the current contribution. Moreover, when the ion concentration is very high (such as in solvent-free electrolyte systems), the potential gradient in the bulk electrolyte is not zero. The remaining electric potential remains in the system even after the EDLs are formed. Therefore, the effect of an external electric field should be taken into consideration in the principle of ECL devices, especially when the concentrations of the radical ions are high and the thickness of the emission layer is very small, which is typical in ECL displays.

In this paper, we systematically investigated the mass transport of electro-active species in gel electrolytes and the related emission mechanisms using experiments and simulations. The dependence of the device performance on the applied voltage and frequency was also examined. Because practical displays require the emission of red (R), green (G), and blue (B) light, we determined the optimal conditions of RGB emissions on the basis of the working mechanisms.

Results and discussion

The chemical structures of the materials used in this study are shown in Fig. 1. We categorized the luminophores into three types according to the radical ion formed by the redox reactions: generating $A^{\bullet 3+}$ and $A^{\bullet +}$ from A^{2+} ($Ru(bpy)_3Cl_2$ and $Ru(bpy)_3(PF_6)_2$, type I), $A^{\bullet 2+}$ and $A^{\bullet}$ from A^{1+} ($Ir(diFppy)_2(bpy)PF_6$, type II), and $A^{\bullet +}$ and $A^{\bullet -}$ from A^0 (DPA, type III). Each type shows different long-distance movement behavior of the radical ions: all ions move toward the same direction (type I), oxidized and initial ions move toward the same direction, but the reduced ions are not affected (type II), and the radical ions move toward opposite directions but the initial molecules are not affected (type III). Thus, the emission behaviors should be understood according to the type of luminophore.

The impact of the long-distance migration in the ECL device under an electric field was investigated using electrochemical impedance spectroscopy (EIS) and light emission decay of the ECL devices. Fig. 2a presents Nyquist plots for the ECL gel, including $Ru(bpy)_3Cl_2$. The other Nyquist plots for the $Ru(bpy)_3(PF_6)_2$, $Ir(diFppy)_2(bpy)PF_6$, and DPA gels are provided in the ESI (Fig. S1a–c†). The gels were sandwiched between two indium-tin-oxide (ITO)-coated glasses with a 60 μm-thick spacer. An imperfect capacitance model with equivalent circuits containing constant phase elements (CPEs) can be used to characterize the behaviors.[24,25]

The equivalent circuit model is depicted in the inset of Fig. 2b. The model includes CPEs in parallel for the interface between the electrode and electrolyte (constant phase element of the double layer $CPE_{DL} = Q_{DL}(i\omega)^{\alpha_{DL}}$) and that between the electrode and the redox species (pseudocapacitance element, $CPE_{PC} = Q_{PC}(i\omega)^{\alpha_{PC}}$). The model is expressed as:

$$Z(\omega) = R_s + \frac{1 + R_{ct}Q_{PC}(i\omega)^{\alpha_{PC}}}{Q_{PC}(i\omega)^{\alpha_{PC}} + Q_{DL}(i\omega)^{\alpha_{DL}}(1 + R_{ct}Q_{PC}(i\omega)^{\alpha_{PC}})} \quad (1)$$

where R_s and R_{ct} are the solution resistance and charge transfer resistance, respectively. The CPE parameter Q represents the admittance of the interface at $\omega = 1$ rad s^{-1} and α is the exponent of the complex frequency (ω). The exponents $\alpha = 1$ and $\alpha = 0$ correspond to an ideal capacitor and a resistor, respectively. The evaluated model parameters of the Nyquist plots for the ECL gels are summarized in the ESI (Tables S1–S4†). Fig. 2b exhibits the potential-dependence of the characteristic parameters of CPE_{DL}, CPE_{PC}, α_{DL}, and α_{PC} from the $Ru(bpy)_3Cl_2$ gel. Although the CPE_{DL} value remained similar, the CPE_{PC} value increased rapidly at 3 V_{pp} because of redox reactions. The α_{DL} value (0.9) did not change significantly over the entire potential range, implying that the response of the electrolyte is similar to that of an ideal capacitor. On the contrary, α_{PC} had lower values (0.67 at 20 mV_{pp}) and gradually decreased to 0.49 at 4 V_{pp}, which indicates that the redox ions made the gel an incomplete capacitor. The results became more prominent with increasing potential. Fig. S1d–f in the ESI† shows the characteristic parameters of the other ECL gels.

Fig. 3a–d shows the transient emission profiles in a top–bottom electrode setup. The $Ru(bpy)_3Cl_2$ gel (Fig. 3a) was sandwiched between two identical ITO electrodes and an operating voltage of 5.0 V_{pp} was applied. The light intensity profiles from the $Ru(bpy)_3Cl_2$ gel at low frequencies (50 Hz) had a shoulder at ~2.0 ms after a potential was applied. The shoulder became more prominent at a lower frequency (30 Hz).

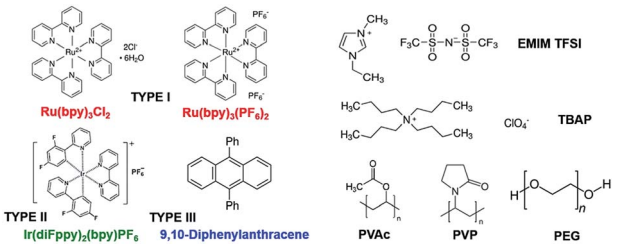

Fig. 1 Chemical structures of the ECL materials: $Ru(bpy)_3Cl_2$, $Ru(bpy)_3(PF_6)_2$, $Ir(diFppy)_2(bpy)PF_6$, and DPA for the red, red, green, and blue ECL luminophores, respectively. Ionic liquids [EMIM][TFSI] and TBAP are used as electrolytes. Three polymers are used as gelation materials: PVAc for red, PVAc and PEG for green, and PVAc and PVP for blue ECL gels.

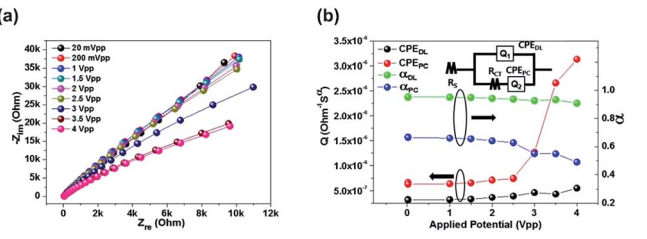

Fig. 2 Electrochemical impedance spectroscopy results. (a) Nyquist plots of the $Ru(bpy)_3Cl_2$ gel as a function of the applied voltages. (b) Fitted CPE parameters extracted from the Nyquist plots in (a), and the inset corresponds to the equivalent circuit model of the device.

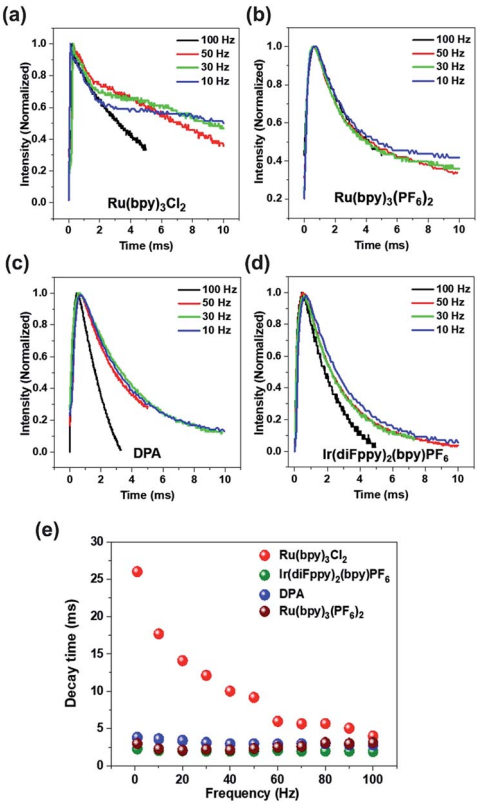

Fig. 3 (a–d) Transient light emission profiles of $Ru(bpy)_3Cl_2$, $Ru(bpy)_3(PF_6)_2$, DPA, and $Ir(diFppy)_2(bpy)PF_6$ gels at various operating frequencies. (e) Summary of the emission decay times (the time at which the light intensity becomes half that of the maximum) of the ECL devices containing $Ru(bpy)_3Cl_2$, $Ir(diFppy)_2(bpy)PF_6$, DPA, and $Ru(bpy)_3(PF_6)_2$ at the applied voltages of 5, 5.8, 6.5, and 5 V_{pp}, respectively, at various operating frequencies.

Fig. 3b compares the transient emission profiles of the $Ru(bpy)_3(PF_6)_2$ gel under identical conditions. In contrast to the $Ru(bpy)_3Cl_2$ gel, the emission profile of the $Ru(bpy)_3(PF_6)_2$ gel did not have a shoulder at 30 Hz and a small shoulder peak appeared at 10 Hz. The transient emission profiles of the $Ir(diFppy)_2(bpy)PF_6$ and DPA gels did not show any shoulder even at lower frequencies (Fig. 3c and d). Fig. 3e summarizes the frequency dependence of decay times. The $Ru(bpy)_3Cl_2$ gel showed a continuous increase in decay time (2 ms at 100 Hz to 25 ms at 1 Hz) as the frequency decreased, but the decay time of the other gels remained constant as the frequency decreased.

The relatively longer decay time of the $Ru(bpy)_3Cl_2$ gel at low frequencies suggests that the annihilation process occurs not only due to the ECL luminophores being located near the electrode but also due to the luminophores moving a long distance. In contrast, the decay times of the gels containing the other luminophores were frequency-independent, which implies that the long-distance movement is not effective and light emission takes place mainly among the radical ions near the electrodes. Note that the frequency-independence of the light decay does not exclude the possibility of the long-distance movement. The contribution of the long-distance movement may increase with a higher ion velocity under a stronger electric field. Because the $Ru(bpy)_3Cl_2$ and $Ru(bpy)_3(PF_6)_2$ gels have identical compositions and cations, the differences in the decay times and EIS results may originate from the mobility difference. The heavier counter ions (PF_6^-) in $Ru(bpy)_3(PF_6)_2$ decrease the mobility of the cations,[10] so light emission takes place mainly in the diffusive region under operational conditions. The appearance of the shoulder peak at 10 Hz for the $Ru(bpy)_3(PF_6)_2$ gel implies that the long-distance movement becomes effective due to the longer time available for movement.

Fig. 4a–c illustrates the effect of the long-distance movement in the $Ru(bpy)_3Cl_2$ gel on the annihilation process. $Ru(bpy)_3^{2+}$ should be uniformly distributed in the gel before the application of an external voltage. When the applied potential is high enough to generate a large amount of radical ions, the $Ru(bpy)_3^{2+}$ ions are converted to $Ru(bpy)_3^{\cdot 1+}$ at the negative electrode (cathode) and to $Ru(bpy)_3^{\cdot 3+}$ at the positive electrode (anode) (Fig. 4a). The cationic $Ru(bpy)_3^{2+}$ accumulates at the cathode, resulting in a higher concentration of $Ru(bpy)_3^{\cdot 1+}$ than $Ru(bpy)_3^{\cdot 3+}$ at the anode. When the voltage direction is switched (Fig. 4b), a large amount of $Ru(bpy)_3^{\cdot 3+}$ is generated at the anode and quickly reacts with the pre-formed $Ru(bpy)_3^{\cdot 1+}$, from which strong but short-term luminescence is observed. On the other hand, the remaining excess $Ru(bpy)_3^{\cdot 3+}$ ions are distributed toward the bulk because of the electric field and the electrostatic repulsion from the anode. Although a lower concentration of $Ru(bpy)_3^{\cdot 1+}$ ions is produced at the cathode, the conversion from the approaching $Ru(bpy)_3^{2+}$ to $Ru(bpy)_3^{\cdot 1+}$ proceeds continuously. Accordingly, the emission at the cathode is weak, but remains longer, as long as the $Ru(bpy)_3^{\cdot 3+}$ ions are fed from the bulk. When the voltage direction is switched again (Fig. 4c), the $Ru(bpy)_3^{\cdot 1+}$ ions are generated again at the cathode and react with $Ru(bpy)_3^{\cdot 3+}$, producing a strong emission. The emission continues because the pre-formed $Ru(bpy)_3^{\cdot 3+}$ ions migrate to the cathode. At the anode, the emission is weak and short-lived, since the emission reaction takes place only at the electrode without the supplement of $Ru(bpy)_3^{\cdot 3+}$. The effect of the long-distance migration on light emission is further supported by an experimental setup with horizontally patterned ITO electrodes (Fig. 4d). The purpose of this experiment is the visual observation of whether the emission occurs sequentially or simultaneously in the electrodes. For clearer detection, we designed an electrode gap of ~100 μm, which is slightly thicker than the spacer (~60 μm) used in a top–bottom configuration. Fig. 4e and f show the temporal changes in emission during a cycle of potential switching. The emission at the anode is strong, but dims quickly; in contrast, the emission at the cathode is weak but maintained for a longer time (see Movie S1†). After switching the voltage direction (Fig. 4f), the emission at the cathode is intense and long, whereas that at the anode is weak and short. These results are in good consistency with the schematic illustrations in Fig. 4b and c.

Fig. 5a–d exhibits the ECL emissions from the $Ru(bpy)_3Cl_2$ gel (a), the $Ru(bpy)_3(PF_6)_2$ gel (b), the $Ir(diFppy)_2(bpy)PF_6$ gel (c), and the DPA gel (d) in the horizontal ITO-electrode setup at wider ranges of frequency (≤30 Hz) and voltage. For the $Ru(bpy)_3Cl_2$ gel, sequential emission was observed at low

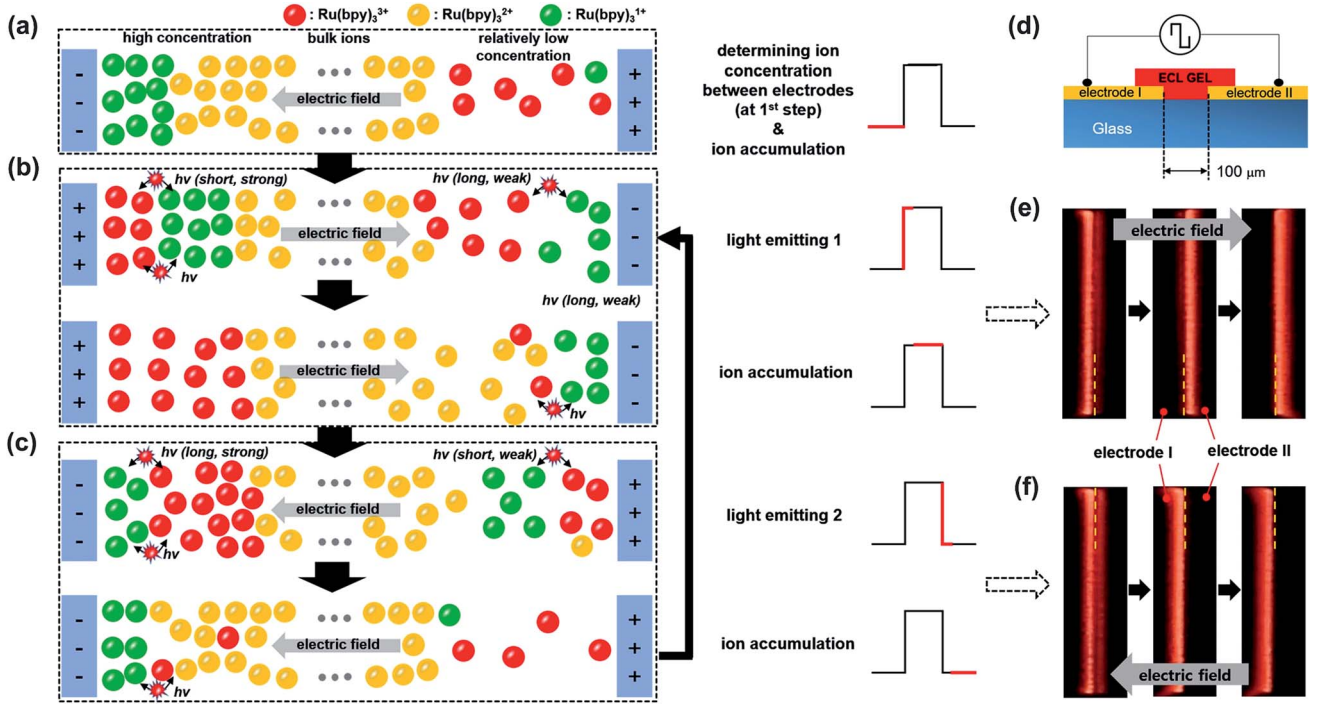

Fig. 4 Schematic illustration of the long-distance migration effect of $Ru(bpy)_3Cl_2$ and experimental verification. (a–c) Distribution of radical ion concentration and luminescence behaviors at each stage: (a) the concentration gradient built up according to the electric field, (b) light emission induced by a switching potential and different emission behaviors at each electrode due to a pre-distributed luminophore concentration, and (c) light emission by another switching potential and different emission behavior at the electrodes. (d) Schematic illustration of horizontally patterned ITO electrodes. (e and f) Digital images of light emission on the horizontally patterned ITO electrode setup. The emission is taken during one cycle at an applied frequency and voltage of 5 Hz and 5.6 V_{pp}, respectively.

frequencies (≤10 Hz) and low voltages (≤5.2 V_{pp}) (Movie S1†), whereas simultaneous emission was observed at higher frequencies and voltages. The sequential and simultaneous emissions are denoted as ▯▯ and ■, respectively. Their snapshots are captured in Fig. 5a. The sequential emission at low V_{pp} for the $Ru(bpy)_3Cl_2$ gel is attributed to the low concentration of radical ions. When the migration period of $Ru(bpy)_3^{\bullet 3+}$ is short at high frequencies or when the voltage is large enough to generate a large amount of radical ions, the emissions at the electrodes follow the schematic illustrations in Fig. 4b and c. On the other hand, if the concentration of $Ru(bpy)_3^{\bullet 3+}$ is low due to a small applied voltage, $Ru(bpy)_3^{\bullet 3+}$ ions are depleted near the anode, resulting in sequential emission. In the case of the $Ru(bpy)_3(PF_6)_2$ gel, because of the relatively short migration distance compared to that of the $Ru(bpy)_3Cl_2$ gel, the simultaneous emission occurred at higher frequencies and voltages (Fig. 5b and Movie S2†). For the $Ir(diFppy)_2(bpy)PF_6$ gel, sequential emission was observed regardless of the frequency (≤30 Hz) and voltage (Fig. 5c). As the voltage is applied, the positively charged $Ir(diFppy)_2(bpy)^{\bullet +}$ accumulates. Since the neutral $Ir(diFppy)_2(bpy)^{\bullet 0}$ reduced at the cathode does not respond to the electric field, the emission takes place only at the anode after switching the voltage. The emission was strong and short, and completely sequential with the same emission profile. Images of the sequential emission are provided in Fig. 5c and a Movie in the ESI (Movie S3†). The light emission of the device containing DPA also showed only sequential emission except at very low frequencies (≤1 Hz) (Fig. 5d and Movie S4†). Sequential emission for the DPA gel is likely due to the short lifetime of the anion radical in the NMP solvent.[26] The annihilation takes place only at the cathode where new DPA anion radicals are generated.

While the horizontal electrode setup made visual observation of the emission process possible, the analysis of ECL behavior at higher frequencies was not available due to limited camera performance. Therefore, we used a top–bottom configuration with larger active areas and thus higher currents, because these short and long emission behaviors originating from ion migration of the luminophores can also be characterized by transient current profiles. Fig. 6a–c displays the transient current profiles of the ECL devices at various operating frequencies (30, 50, 100, and 500 Hz). The operating voltages were 6 V_{pp} for the red current profile (a), 7 V_{pp} for the green current profile (b), and 8 V_{pp} for the blue current profile (c). These voltages were chosen because they should be sufficient to turn on the light but were not too high, so that the devices could maintain the same emission intensity for more than 5 min. Fig. 6a–c shows the 1st and the 2nd current profiles in each emission cycle, denoted in the insets of the left column figures (30 Hz). The 2nd current profile was inverted so that it could be compared with the first one. The current profiles at lower voltages are shown in Fig. S4–S6.† Asymmetric current profiles were recorded from the gel containing $Ru(bpy)_3Cl_2$ at low operating frequencies (30 and 50 Hz) as described in Fig. 4.

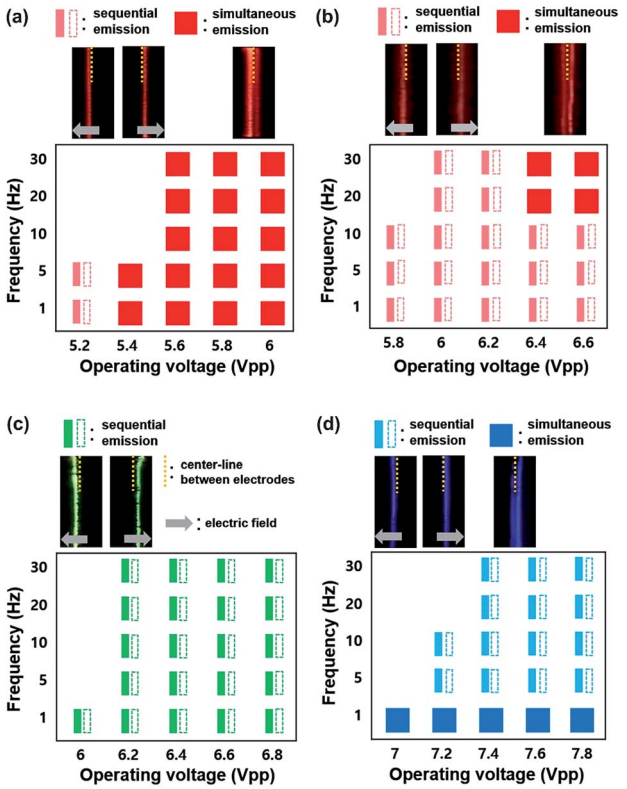

Fig. 5 Dependence of light emission responses of the $Ru(bpy)_3Cl_2$, $Ru(bpy)_3(PF_6)_2$, $Ir(diFppy)_2(bpy)PF_6$, and DPA gels at various low operating frequencies (≤30 Hz) and voltage conditions. The sequential and simultaneous emissions are denoted as ▯ and ■, respectively. (a) A sample of the $Ru(bpy)_3Cl_2$ gel exhibiting both sequential and simultaneous emission. (b) A sample of the $Ru(bpy)_3(PF_6)_2$ gel exhibiting both sequential and simultaneous emission at high operating frequencies and voltages. (c) A sample of the $Ir(diFppy)_2(bpy)PF_6$ gel showing only sequential emission. (d) A sample of the DPA gel showing sequential emission except at very low operating frequencies (1 Hz).

The asymmetric behavior disappeared at high frequencies because the fast alternating electric field reduces the migration distance of the ions. The current profiles in type II (green, $Ir(diFppy)_2(bpy)PF_6$) and type III (blue, DPA) showed symmetric profiles regardless of the operating frequencies, which supports the idea that the migration of the ions does not affect ECL behavior.

Fig. 7a–c shows the transient emission profiles of the $Ru(bpy)_3Cl_2$ gel (a), the $Ir(diFppy)_2(bpy)PF_6$ gel (b), and the DPA gel (c). The operating voltages were 5.5 V_{pp} for the red emission, 5.8 V_{pp} for the green emission, and 6.5 V_{pp} for the blue emission. The frequency was in the range of 50–1000 Hz. The $Ru(bpy)_3Cl_2$ gel and the DPA gel exhibited asymmetric light emission profiles in each period at all frequencies, whereas the $Ir(diFppy)_2(bpy)PF_6$ gel maintained symmetric emission profiles at all frequencies. Fig. 7d summarizes the frequency-dependence with normalized light intensities. The optimal operating frequencies were 200 Hz, 600–700 Hz, and 400–500 Hz for the red, green, and blue ECL gels, respectively. The light intensity per unit time was calculated by integrating the area under the curves and multiplying it by the operating frequency. The calculated intensities are in good agreement with the measured values, as shown in Fig. S3.†

For an electrolyte system, the changes in the ion concentrations and the potential difference are often described by the modified Poisson–Nernst–Planck (mPNP) equation. Since the electrolyte system in this study is a solvent-free pure electrolyte, we used a more generalized mPNP equation (eqn (2)) proposed by Lee *et al.*[27] The equation predicts the decrease of the ion mobility matrix in a concentrated ionic system compared to a dilute ionic system. Eqn (2) was solved with Poisson's equation (eqn (3)) to obtain the potential change of the electrolyte system.

$$\frac{\partial c_i}{\partial t} = D\nabla\left(c_i\left(1 - N_A\sum_{i=1}^{n} a_i^3 c_i\right)\nabla\frac{z_i e\phi}{k_B T} + \left(1 - N_A\sum_{i=1}^{n} a_i^3 c_i\right)\nabla c_i + N_A a_i^3 c_i \sum_{i=1}^{n}\nabla c_i\right) \quad (2)$$

$$-\varepsilon\varepsilon_0\nabla(\nabla\phi) = \rho = F\sum_{i=1}^{n} z_i c_i \quad (3)$$

where N_A: Avogadro's number, c_i: ion concentration [M] of species i, a_i: ion size of ion species i, z_i: valence number of species i, e: the elementary charge, k_B: Boltzmann constant, T: the temperature, ϕ: electric potential, and F: Faraday constant.

The ECL system in this study contains two chemical reactions: (1) the redox reactions at the electrodes (the formation of $Ru(bpy)_3^{\bullet 1+}$ and $Ru(bpy)_3^{\bullet 3+}$), and (2) the recombination of the redox radicals. In order to clearly understand the ion distributions under external potentials and the chemical reactions, we first solved the equations under DC conditions where the redox reactions take place but the recombinations do not happen. Then, we solved the equations under AC conditions where the recombination reaction was also included.

COMSOL Multiphysics 5.3 (COMSOL, Inc.) was used for the simulation. One dimensional ionic motions were assumed in the calculations, which is usual in tracking the motions driven by external electric fields. In addition, to simplify the calculations, the size of all ions is considered to be the same. With the consideration of the molecular volume of [EMIM][TFSI], the size of 0.55 nm was used for each ion.[28] The initial weight fraction of $Ru(bpy)_3Cl_2$ was 5.0 wt% in the [EMIM][TFSI] electrolyte, which corresponds to 3.12 mol% of $Ru(bpy)_3^{2+}$ in the total cation concentration. The initial concentrations of ions and the maximum concentration that all ions can reach are given in Table S5 (ESI†), in which the maximum ion concentration (9.981 M) was calculated on the basis of the size of the ions.[29] In general, the maximum concentration of cations or anions near the electrode is considered as less than twice of the total ion concentration in the bulk ionic liquid,[30] so the suggested maximum ion concentration is acceptable. The thickness of the electrolyte layer was 100 μm, and the anode (right electrode) voltage was 3 V higher than the cathode (left electrode) voltage. We assumed that the redox reactions exclusively take place

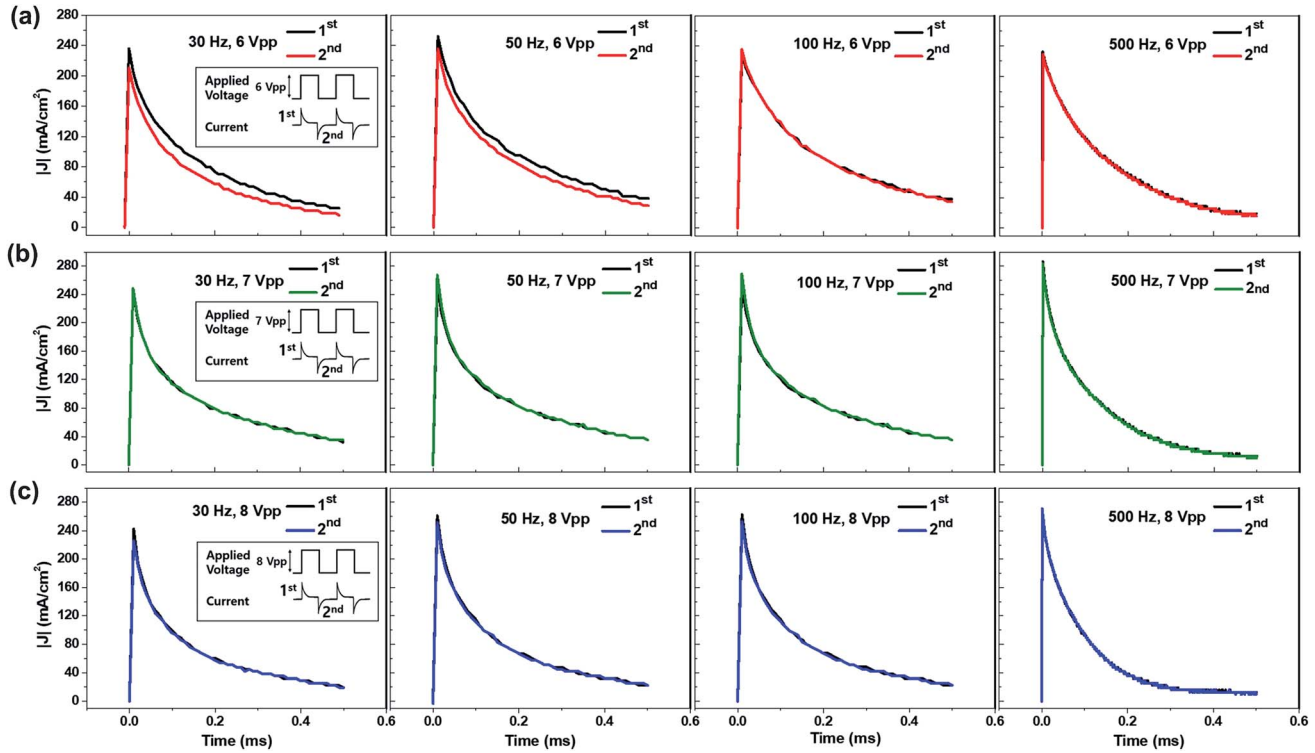

Fig. 6 Comparisons of the transient current profiles at various operating frequencies (30, 50, 100, and 500 Hz) of the ECL gels with different dyes: (a) $Ru(bpy)_3Cl_2$, (b) $Ir(diFppy)_2(bpy)PF_6$, and (c) DPA. The insets in the left column represent the operation cycles. The 1st and 2nd current profiles are the operation cycle of each gel. The 2nd profiles were inverted so that they could be compared with the 1st current profiles.

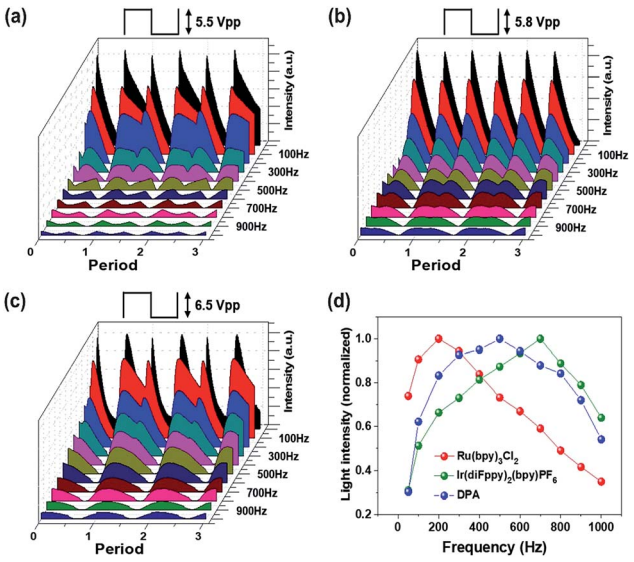

Fig. 7 (a–c) Transient light emission responses of the $Ru(bpy)_3Cl_2$ gel (a), the $Ir(diFppy)_2(bpy)PF_6$ gel (b) and DPA gel (c) based devices at 5.5, 5.8, and 5.6 V_{pp}, respectively. The operating frequency was in the range of 50–1000 Hz. The gel dimensions were 5 mm in diameter and 60 μm in thickness. (d) Frequency dependence of the normalized light intensities of the $Ru(bpy)_3Cl_2$, $Ir(diFppy)_2(bpy)PF_6$, and DPA-containing ECL gel devices.

when the electric field is higher than 3 V/100 μm and only within the electric double layer (EDL) near the electrodes, and they are first order reactions (namely, $k_1[Ru(bpy)_3^{2+}]$ with $k_1 = 2.23 \times 10^5\ s^{-1}$ for both reduction and oxidation reactions. Note that the reaction constant was calculated empirically (considering 30% conversion in 1.0 μs). The recombination reaction was considered as a second order reaction, $k_2[Ru(bpy)_3^{\bullet 1+}][Ru(bpy)_3^{\bullet 3+}]$, with a recombination reaction constant k_2 of $10^{10}\ M^{-1}\ s^{-1}$. The k_2 value was obtained from a reported annihilation reaction constant of $Ru(bpy)_3^{2+}$.[31]

Fig. 8 shows the simulation results under DC conditions including only the redox reactions without recombination. Temporal changes of the potential across the two electrodes are represented in Fig. 8a. Upon the application of an electric potential between the electrodes, EDLs were formed at the electrodes and induced abrupt potential changes (see the vertical lines in Fig. 8a). The linear potential gradients across the bulk ion gel were estimated, in which the slope decreased with time. In general, the formation of an EDL is completed in the order of microseconds,[27,29,32–34] so that the potential in the bulk electrolyte is negligible in a time scale of milliseconds after applying an electric field. However, the simulation results indicate that the EDL formation is slow and the electric field along the gel gradually decreases but does not fully disappear as shown in Fig. 8b (43.3 mV/100 μm after 10 ms), when the concentrated ionic system involves redox reactions. It is a notable result different from the conventional concept in dilute electrolyte systems. This remaining electric field may lead to the long distance migration of ions along the ion gel, supporting the long tail in the current of the ECL gel (ESI Fig. S7†). Another important point is that the potential drops at the

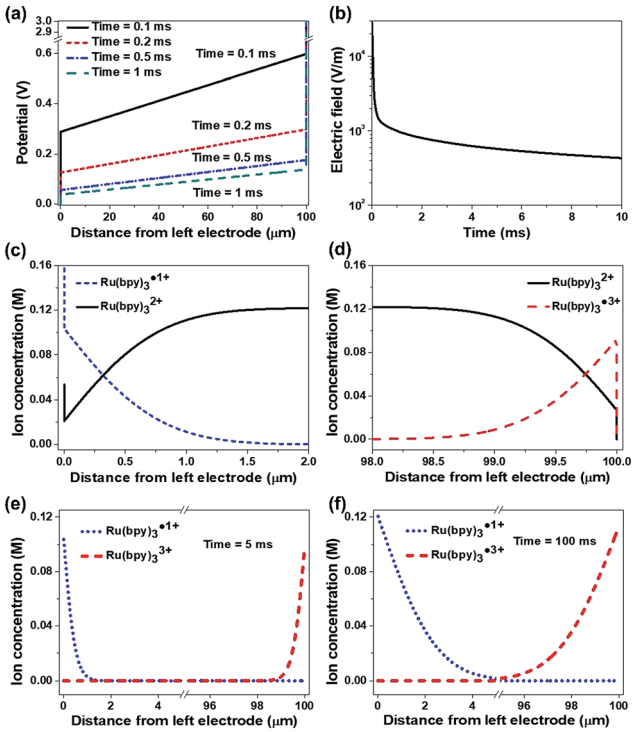

Fig. 8 The simulation results obtained for the ECL gel containing $Ru(bpy)_3Cl_2$ under DC electric field conditions, which include the redox reaction but not the recombination reaction. The thickness of the gel is 100 μm and the potential difference between the cathode (left) and the anode (right) is 3 V. (a) The potential changes in the gel in 0.1 ms, 0.2 ms, 0.5 ms, and 1 ms after applying the potential. (b) The electric field at the center of the gel as a function of time. (c) The density of $Ru(bpy)_3^{\bullet 1+}$ and $Ru(bpy)_3^{2+}$ near the cathode after 10 ms. (d) The density of $Ru(bpy)_3^{2+}$ and $Ru(bpy)_3^{\bullet 3+}$ near the anode after 10 ms. (e and f) Time dependent ion concentration profiles of $Ru(bpy)_3^{2+}$ and $Ru(bpy)_3^{\bullet 3+}$ after 5 ms and 100 ms.

electrodes by the EDLs are not symmetric. An electrolyte containing cations with a larger valence number induces a smaller potential drop at the cathode than at the anode even without redox reactions (ESI Fig. S8†). This asymmetric potential drop becomes more considerable when the electrolyte undergoes a redox reaction. Fig. 8c and d exhibit the concentration distributions of the reactive ions near the electrodes in 10 ms after the potential is applied. The ion distribution indicates abrupt concentration changes within the EDL (~1 nm apart from the electrodes). Fig. 8e and f compare the distributions of $Ru(bpy)_3^{\bullet 1+}$ and $Ru(bpy)_3^{\bullet 3+}$ near the electrodes after 5 ms (Fig. 8e) and 100 ms (Fig. 8f). The amount of $Ru(bpy)_3^{\bullet 1+}$ ions was greater than that of $Ru(bpy)_3^{\bullet 3+}$ ions, and the difference became greater as the duration of the voltage application increased.

Fig. 9 shows the dynamic ion concentration distributions under AC conditions in which the recombination reaction is added. We applied the electric field obtained in Fig. 8a to eqn (2), and tracked the ion flux during alternate potential switches. We compare the results in the 5th cycle at a low frequency (5 Hz). Fig. 9a and b exhibit the first half period and Fig. 9c and d represent the next half period. At the beginning of the periods,

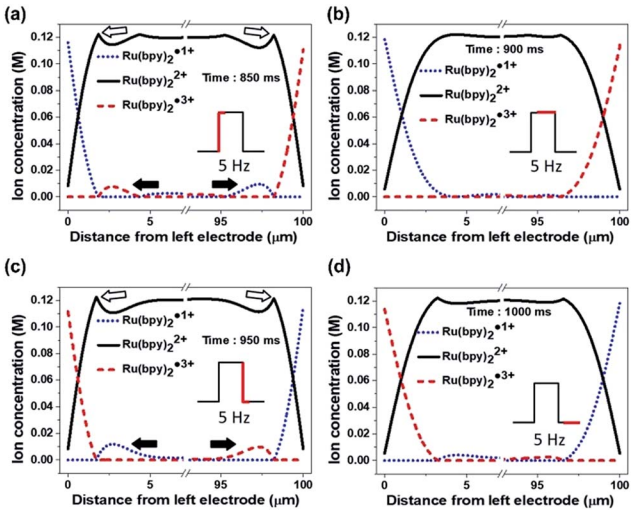

Fig. 9 Simulation results for the ion concentration profiles of the active ions at the 5th cycle under an AC electric field dynamic situation which includes both the redox reaction and the recombination reaction. The AC frequency is 5 Hz. The times indicated in the figures are the time spans after applying the AC cycles. (a and b) The concentration profiles at the beginning of the first half cycle (a) and at the end of the first half cycle (b). (c and d) The concentration profiles at the beginning of the second half cycle (c) and at the end of the second half cycle (d).

the concentrations of both $Ru(bpy)_3^{\bullet 1+}$ and $Ru(bpy)_3^{\bullet 3+}$ decreased and spanned a relatively wide range (~1.9 μm) from the cathode and anode, respectively, and the profiles also showed satellite hills (indicated with solid arrows) near the opposite electrode (see Fig. 9a and c). The concentration profiles and the hills are the sources of the recombination reaction. The concentration of the recombination product (namely, unexcited $Ru(bpy)_3^{2+}$) peaked near where the concentration profile of $Ru(bpy)_3^{\bullet 1+}$ and the hill of $Ru(bpy)_3^{\bullet 3+}$ met, and *vice versa* (see empty arrows in Fig. 9a and c). In comparison with the profiles in Fig. 9b, the hills in Fig. 9d were maintained for longer, which implies longer light emission in the second half period. The results in the 5th cycle at a higher frequency (50 Hz) are also provided (see Fig. S9†). The concentration profiles at higher frequency had ion distributions within smaller distances (<1 μm) and smaller hills. They also exhibited an asymmetric distribution of hills in the first and second half periods, but the difference was smaller. Overall, the light emission at a low frequency is longer and more asymmetric than that at a high frequency.

Fig. 10a–c shows luminance *versus* applied voltage with various luminophore concentrations. The luminance of the ECL devices became larger as the luminophore concentration increased. The selected concentrations of the ECL luminophores for the devices were the saturation values without precipitation for several days. The ECL devices were fabricated using a nozzle printer on a Pt/Si substrate then covered with ITO/glass as a top electrode. The maximum luminance properties for the red, green, and blue ECL devices are 232.4 Cd m^{-2} at 5.2 V_{pp}, 123.5 Cd m^{-2} at 5.4 V_{pp}, and 60.2 Cd m^{-2} at 6.4 V_{pp},

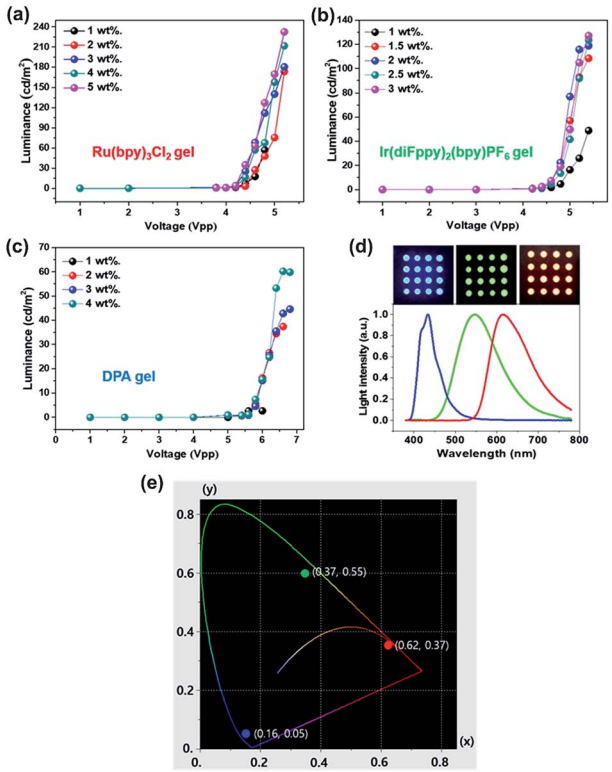

Fig. 10 (a–c) Luminance *versus* applied voltage and luminophore concentrations of $Ru(bpy)_3Cl_2$, $Ir(diFppy)_2(bpy)PF_6$ and DPA gels at an operating frequency of 500 Hz. (a) $Ru(bpy)_3Cl_2$ gel at a concentration of 1 to 5 wt%, (b) $Ir(diFppy)_2(bpy)PF_6$ gel at a concentration of 1 to 3 wt%, and (c) DPA gel at a concentration of 1 to 4 wt%. (d) The emission spectra of the $Ru(bpy)_3Cl_2$, $Ir(diFppy)_2(bpy)PF_6$, and DPA gels, and camera images of the 4 × 4 arrays. (e) CIE color coordinates demonstrated in this study: $(x, y) = (0.62, 0.37)$ for red, (0.37, 0.55) for green, and (0.16, 0.05) for blue.

respectively. The camera images and emission spectra of the fabricated ECL devices are given in Fig. 10d. The CIE coordinates of red, green and blue were $(x, y) = (0.62, 0.37)$, (0.37, 0.55) and (0.16, 0.05), respectively (Fig. 10e). The dot arrays (diameter = 2 mm) were prepared using a nozzle printer on the ITO/glass substrate as a top electrode. The wavelengths at the maximum intensity are 615, 545, and 430 nm for the red, green, and blue colors, respectively.

Conclusion

This study reveals that the radical ions generated by redox reactions at the electrodes of an ECL device can move a long distance, which is different from the conventional concept that neglects the long-distance migration of electro-active ion species. The experimental results are consistent with theoretical simulations. In a highly concentrated electrolyte system with redox reactions, the potential drops through the EDLs, but the potential gradient in the bulk electrolyte is not zero and has a long-lasting remaining potential. This remaining potential results in long-distance migration of ECL luminophores. Several factors such as the type of radical ion and counter ion, operating frequency, and applied voltage determine the movement distance of the radical ions. Using a parallel electrode setup, we found that simultaneous emission on both electrodes is observed when the ions move toward the same direction (type I), while sequential emission is detected when the ions are weakly affected by the electric field (type II) or move to opposite directions under an AC electric field (type III). The effect of long-distance migration is valid at low frequencies (<50 Hz) but not at high frequencies. Understanding the ion movements in ECL gel systems helped determine the optimal operating conditions (*e.g.* voltage and frequency) for RGB colors.

Author contributions

S. S. and U. J. designed the research. S. S. performed the experiments. Y. P. and I. K. performed computational simulations. S. C. and I. Y. participated in the sample preparation. S. S., Y. P., H. C. M. and U. J. analysed the experimental data, discussed the results, and wrote the manuscript. S. S. and Y. P. contributed equally to this study.

Conflicts of interest

There are no conflicts to declare.

Acknowledgements

This work was supported by the Samsung Research Funding Center of Samsung Electronics under Project Number SRFC-MA1301-07.

References

1 S. W. Feldberg, *J. Am. Chem. Soc.*, 1966, **88**, 390.
2 J. Maloy and A. J. Bard, *J. Am. Chem. Soc.*, 1971, **93**, 5968.
3 A. J. Bard, *Electrogenerated chemiluminescence*, Marcel Dekker, New York, 2004.
4 M. M. Richter, *Chem. Rev.*, 2004, **104**, 3003.
5 R. Pyati and M. M. Richter, *Annu. Rep. Prog. Chem., Sect. C: Phys. Chem.*, 2007, **103**, 12.
6 R. J. Forster, P. Bertoncello and T. E. Keyes, *Annu. Rev. Anal. Chem.*, 2009, **2**, 359.
7 Z. Liu, W. Qi and G. Xu, *Chem. Soc. Rev.*, 2015, **44**, 3117.
8 N. Itoh, *Materials*, 2010, **3**, 3729.
9 P. Burrows, V. Bulovic, S. Forrest, L. S. Sapochak, D. McCarty and M. Thompson, *Appl. Phys. Lett.*, 1994, **65**, 2922.
10 M. Buda, G. Kalyuzhny and A. J. Bard, *J. Am. Chem. Soc.*, 2002, **124**, 6090.
11 G. Kalyuzhny, M. Buda, J. McNeill, P. Barbara and A. J. Bard, *J. Am. Chem. Soc.*, 2003, **125**, 6272.
12 E. S. Handy, A. J. Pal and M. F. Rubner, *J. Am. Chem. Soc.*, 1999, **121**, 3525.
13 H. C. Moon, T. P. Lodge and C. D. Frisbie, *Chem. Mater.*, 2014, **26**, 5358.
14 K. Nishimura, Y. Hamada, T. Tsujioka, S. Matsuta, K. Shibata and T. Fuyuki, *Jpn. J. Appl. Phys.*, 2001, **40**, L1323.

15 T. Nobeshima, T. Morimoto, K. Nakamura and N. Kobayashi, *J. Mater. Chem.*, 2010, **20**, 10630.
16 T. Daimon and E. Nihei, *Materials*, 2013, **6**, 1704.
17 T. Nobeshima, M. Nakakomi, K. Nakamura and N. Kobayashi, *Adv. Opt. Mater.*, 2013, **1**, 144.
18 E. Kerr, E. H. Doeven, G. J. Barbante, C. F. Hogan, D. J. Bower, P. S. Donnelly, T. U. Connell and P. S. Francis, *Chem. Sci.*, 2015, **6**, 472.
19 H. L. Filiatrault, G. C. Porteous, R. S. Carmichael, G. J. Davidson and T. B. Carmichael, *Adv. Mater.*, 2012, **24**, 2673.
20 H. C. Moon, T. P. Lodge and C. D. Frisbie, *J. Am. Chem. Soc.*, 2014, **136**, 3705.
21 H. C. Moon, T. P. Lodge and C. D. Frisbie, *J. Mater. Chem. C*, 2016, **4**, 8448.
22 K. Hong, Y. K. Kwon, J. Ryu, J. Y. Lee, S. H. Kim and K. H. Lee, *Sci. Rep.*, 2016, **6**, 29805.
23 L. Pilon, H. Wang and A. d'Entremont, *J. Electrochem. Soc.*, 2015, **162**, A5158.
24 G. Brug, A. Van Den Eeden, M. Sluyters-Rehbach and J. Sluyters, *J. Electroanal. Chem.*, 1984, **176**, 275.
25 E. Barsoukov and J. R. Macdonald, *Impedance spectroscopy: theory, experiment, and applications*, Wiley-Interscience, Hoboken, NJ, 2005.
26 S. A. Cruser and A. J. Bard, *J. Am. Chem. Soc.*, 1969, **91**, 267.
27 A. A. Lee, S. Kondrat, D. Vella and A. Goriely, *Phys. Rev. Lett.*, 2015, **115**, 106101.
28 A. Elbourne, S. McDonald, K. Voichovsky, F. Endres, G. G. Warr and R. Atkin, *ACS Nano*, 2015, **9**, 7608.
29 L. Pilon, H. Wang and A. d'Entremont, *J. Electrochem. Soc.*, 2015, **162**, A5158.
30 M. V. Fedorov and A. A. Kornyshev, *Chem. Rev.*, 2014, **114**, 2978.
31 M. M. Collinson, R. M. Wightman and P. Pastore, *J. Phys. Chem.*, 1994, **98**, 11942.
32 M. van Soestbergen, *Electrochim. Acta*, 2010, **55**, 1848.
33 X. Jiang, J. Huang, H. Zhao, B. G. Sumpter and R. Qiao, *J. Phys.: Condens. Matter*, 2014, **26**, 284109.
34 R. Morrow, D. R. McKenzie and M. M. M. Bilek, *J. Phys. D: Appl. Phys.*, 2006, **39**, 937.